Crystallization and Structure Determination to 2.5-Å Resolution of the Oxidized [2Fe-2S] Ferredoxin Isolated from *Anabaena* 7120[†]

Wojciech R. Rypniewski,[‡] Deborah R. Breiter,[§] Matthew M. Benning,[‡] Gary Wesenberg,[‡] Byung-Ha Oh,[∥]
John L. Markley,[∥] Ivan Rayment,[‡,∥] and Hazel M. Holden*[‡,§]

*Departments of Chemistry and Biochemistry and the Institute for Enzyme Research, University of Wisconsin—Madison,
Madison, Wisconsin 53705*

Received September 11, 1990; Revised Manuscript Received January 7, 1991

ABSTRACT: The molecular structure of the oxidized form of the [2Fe-2S] ferredoxin isolated from the cyanobacterium *Anabaena* species strain PCC 7120 has been determined by X-ray diffraction analysis to a nominal resolution of 2.5 Å and refined to a crystallographic R factor of 18.7%. Crystals used in this investigation belong to the space group $P2_12_12_1$ with unit cell dimensions of $a = 37.42$ Å, $b = 38.12$ Å, and $c = 147.12$ Å and two molecules in the asymmetric unit. The three-dimensional structure of this ferredoxin was solved by a method that combined X-ray data from one isomorphous heavy-atom derivative with noncrystallographic symmetry averaging and solvent flattening. As in other plant-type [2Fe-2S] ferredoxins, the iron–sulfur cluster is located toward the outer edge of the molecule, and the irons are tetrahedrally coordinated by both inorganic sulfurs and sulfurs provided by protein cysteine residues. The main secondary structural elements include four strands of β-pleated sheet and three α-helical regions.

Iron–sulfur proteins are distributed widely in nature and have been isolated from various sources ranging from bacteria to higher plants and animals. Proteins containing iron–sulfur clusters are indeed numerous and include the high-potential iron–sulfur proteins (HiPIPS), the low-potential ferredoxins, the rubredoxins, aconitase, glutamine amidoribosyltransferase, succinate dehydrogenase, NADH dehydrogenase, nitrate reductase, nitrogenase, and xanthine dehydrogenase, to name but a few (Thomson, 1985). Yet, despite such widespread occurrence, iron–sulfur proteins were generally not recognized as a distinct class of proteins until the 1960's (Beinert, 1973, 1990).

Ferredoxins contain either one or two [4Fe-4S] clusters (or a 3Fe variant of this cluster) or one [2Fe-2S] cluster. It is generally accepted that the [2Fe-2S] ferredoxins from plants and cyanobacteria are primarily involved in photosynthetic electron transport, where they serve as terminal electron acceptors from photosystem I (Trebst & Avron, 1977) or as electron donors in various reactions including the reduction of $NADP^+$ to NADPH (Masaki et al., 1982), reduction of nitrite to ammonia (Ida, 1977), sulfur assimilation (Aketagawa & Tamura, 1980), and glutamate synthesis (Lea & Miflin, 1984). Plant-type ferredoxins display oxidation–reduction potentials between –305 and –455 mV (Cammack et al., 1977). The mechanism by which these proteins modulate the redox potentials of their iron–sulfur prosthetic groups, however, is still not well understood.

The X-ray crystallographic structures of two plant-type ferredoxins isolated from *Spirulina platensis* and *Aphanothece sacrum* are now known to a resolution of 2.5 Å (Tsukihara et al., 1981; Tsutsui et al., 1983). Both proteins display similar molecular folds with approximately 25% of the amino acid residues in a β-pleated sheet and approximately 10% in one

α-helix (Tsukihara et al., 1981; Tsutsui et al., 1983). Another ferredoxin isolated from the *Halobacterium* of the Dead Sea has also been solved crystallographically to a resolution of 2.8 Å and is currently being refined (Sussman et al., 1986).

In this report we describe the crystallization and structure determination to a nominal resolution of 2.5 Å of another [2Fe-2S] ferredoxin isolated from the cyanobacterium *Anabaena* species strain PCC 7120.

EXPERIMENTAL PROCEDURES

Crystallization and Preparation of Heavy-Atom Derivatives. The protein used for this investigation was purified according to the procedure of Oh and Markley (1990). The hanging drop method of vapor diffusion was employed for initial crystallization trials both at room temperature and at 4 °C. Various precipitants were tested including ammonium sulfate, polyethylene glycol 8000, ammonium phosphate, and sodium citrate within the pH range of 5.5–8.0. Only at pH 5.5 could small dark brown needle-like crystals be obtained at both temperatures in the presence of ammonium sulfate. The addition of 1% 2-methyl-2,4-pentanediol to the crystallization experiments was found to yield large single dark brown crystals with typical dimensions of 0.5 mm × 0.5 mm × 1.0 mm. For the investigation described here, crystals were routinely grown in the presence of atmospheric oxygen at 4 °C from 2.6 M ammonium sulfate solutions buffered with 50 mM potassium succinate, pH 5.5. The crystals belong to the space group $P2_12_12_1$ with unit cell dimensions of $a = 37.42$ Å, $b = 38.12$ Å, and $c = 147.12$ Å and two molecules in the asymmetric unit. The maximum resolution of measurable X-ray data is 1.7 Å with a conventional rotating anode X-ray source. A typical precession photograph is shown in Figure 1.

Experiments designed to prepare heavy-atom derivatives were initiated with the crystals grown at pH 5.5, but all attempts to obtain such derivatives failed. The crystals, however, could be transferred to a synthetic mother liquor of 3.76 M ammonium sulfate and 1% 2-methyl-2,4-pentanediol, buffered with 50 mM K^+/Na^+ phosphate, pH 7.5, and at this higher pH one heavy-atom derivative was prepared in the presence of 20 mM trimethyllead acetate. Consequently, all native and

*To whom correspondence should be addressed.
[‡]Institute for Enzyme Research.
[§]Department of Chemistry.
[∥]Department of Biochemistry.

Table I: Intensity Statistics for the Native and Lead Derivative Crystals

	native	$(CH_3)_3Pb$-$OOCCH_3$
no. film packs	99	87
av $R_{sym}{}^a$ (%)	3.8	5.3
av $R_{sca}{}^a$ (%)	2.6	3.1
$R_{merge}{}^a$ (%)	4.5	6.4
total reflections measured	27 168	14 117
independent reflections	7672	6404
resolution (Å)	30–2.5	30–2.5
av isomorphous differences^b (%)	0	19.0
cell dimensions		
a (Å)	37.4	37.3
b (Å)	38.1	37.9
c (Å)	147.1	146.5

$^a R = \sum|I - \bar{I}|/\sum I$; R_{sym} measures the agreement between symmetry-related reflections on the same film, R_{sca} measures the agreement between reflections recorded on successive films in a given film pack, and R_{merge} gives the overall agreement between intensities measured on different films. $^b R = \sum||F_N| - |F_H||/\sum|F_N|$ where $|F_N|$ is the native structure factor amplitude and $|F_H|$ is the derivative structure factor amplitude.

FIGURE 1: 13° precession photograph of the 0*kl* zone. The X-ray photograph was recorded with nickel-filtered copper Kα radiation from a Rigaku RU 200 rotating anode X-ray generator operated at 40 kV and 50 mA with a 200-μm focal cup. The exposure time was 20 h at a crystal-to-film distance of 100 mm.

derivative X-ray data were collected from crystals soaked in a synthetic mother liquor buffered at pH 7.5.

X-ray Data Collection and Processing. X-ray data for the native and the heavy-atom derivative crystals were collected at 4 °C to a nominal resolution of 2.5 Å by the method of oscillation photography. Only one crystal was required per data set. The crystal was rotated about the *a* axis through a net rotation of 90°. The oscillation angle was 1.0° per film pack with an exposure time of 2.1 h and a crystal-to-film distance of 80 mm. X-ray data were collected by using Ni-filtered Cu Kα radiation from a Rigaku RU200 X-ray generator operated at 40 kV and 40 mA with pinhole collimation and a 200-μm focal cup.

The X-ray films were digitized with an Optronics film scanner and processed with a set of programs originally developed by Rossmann (1979) and modified by Schmid et al., 1981. Each film was integrated to 2.5-Å resolution. Partial reflections were added between adjacent film packs. The lead derivative data were scaled to the native X-ray data in shells of equal volume in reciprocal space based on resolution. Each shell of X-ray data, containing approximately 350 reflections, was assigned an individual scale factor. These scale factors ranged from approximately 4.5 for the low-resolution to 11.7 for the highest resolution data. Relevant X-ray data collection statistics may be found in Table I. The native X-ray data set contains 98% of the total theoretical observations to 2.5-Å resolution.

Computational Methods. The positions of the lead binding sites were immediately obvious in a difference Patterson map

calculated at 3.0-Å resolution. It is worth noting that trimethyllead acetate, which proved successful in the structural determination of this ferredoxin, has also been extremely helpful in the X-ray investigations of six other proteins in the laboratory (manuscripts in preparation). The positions and occupancies of the lead binding sites were refined by the program HEAVY (Terwilliger & Eisenberg, 1983) using the origin-removed Patterson-function correlation method (Rossmann, 1960) and are given in Table II.

Protein phases from the lead derivative were calculated with the program HEAVY, and relevant phase calculation statistics are given in Table III. The phasing does not include anomalous scattering information, since film X-ray data are notorious for not yielding a reliable estimate of the anomalous signal. Although the electron density map, phased with the single heavy-atom derivative alone and calculated from 30.0- to 5.0-Å resolution, was noisy, the positions of the iron–sulfur clusters were immediately obvious as the highest peaks in the map. These peaks of electron density exhibited very similar dumbbell shapes, and while the map was not of sufficient quality to trace the course of the polypeptide chain, the electron density corresponding to the iron–sulfur clusters was clearly good enough to determine the relative rotational matrix and the translational vector between the two molecules in the asymmetric unit.

Both the rotational matrix and the translational vector between the two independent molecules in the asymmetric unit were refined with the program MUNCHKINS (developed in the laboratory by G. Wesenberg and I. Rayment). This program

Table II: Refined Heavy-Atom Parameters^a

derivative	site no.	rel. occupancy	x	y	z	B	location
$(CH_3)_3PbOOCCH_3$	1	0.9840	0.4783	0.0699	0.2811	13.8	between side chains of Glu 24 and Glu 32 (monomer 1)
	2	0.7297	0.5063	0.6489	0.0188	24.5	between side chains of Glu 24 and Glu 32 (monomer 2)
	3	0.6563	0.0673	0.3515	0.1071	19.9	interface between monomers

$^a x, y,$ and z are the fractional atomic coordinates; B is the thermal factor in A^2.

Table III: Phase Calculation Statistics

	resolution range (Å)							
	∞–9.11	5.71	4.45	3.77	3.33	3.01	2.77	2.58
no. of reflections	340	646	805	934	1046	1149	1205	1129
figure of merit	0.48	0.42	0.36	0.31	0.32	0.34	0.27	0.17
phasing power [$(CH_3)_3PbOOCCH_3$]^a	1.53	1.67	1.52	1.47	1.52	1.50	1.40	1.11

^{a}The phasing power is the ratio of the root-mean-square heavy-atom scattering factor amplitude to the root-mean-square lack of closure error.
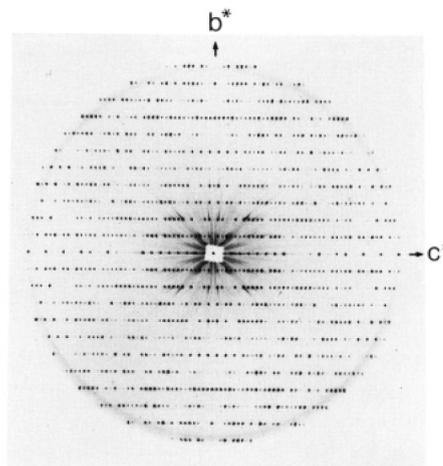
allows the relative orientation and position of two molecules to be determined by searching the three rotational and the three translational degrees of freedom for a maximum fit between the electron density of the two molecules within the asymmetric unit. It is a space group independent program that can be used to find the relationship between two molecules either in the same cell or in different crystal systems. In addition, it allows the superposition of an envelope on the electron density to provide a better definition of the search model. In the initial stages the correlation coefficient between the two molecules in the asymmetric unit was determined for a 9-Å radius sphere of electron density centered around each metal cluster by using as the search model those points in the electron density that were above one σ of the root-mean-square value of the electron density. This constituted approximately half of the points within the sphere of electron density. Since the electron density immediately surrounding the [2Fe-2S] cluster was expected to be 4-fold symmetric, those points of electron density within a radius of 4.5 Å of the center of the metal cluster were excluded from the search in order to remove any ambiguity. Variations of the radius of the search sphere and electron density cutoff did not significantly change the resultant transformation matrix or indicate any other solution. Based on the resultant rotational and translational matrices obtained from MUNCHKINS, the correlation coefficient between the electron density surrounding the [2Fe-2S] clusters in the asymmetric unit was 0.42 whereas the next highest peak in the full rotational search was only 0.28. By using this type of analysis, an unambiguous correlation between the electron density associated with the two iron–sulfur clusters was obtained, and the necessary rotational and translational matrices for molecular averaging were determined. An "averaged" electron density map allowed for unambiguous placement of the iron–sulfur cluster and amino acid residues within the near vicinity of the metal cluster. However, the electron density map was still not of sufficient quality to completely trace the polypeptide chain.

Since it was expected that the ferredoxins isolated from *Anabaena* and *Spirulina* would have similar overall molecular shapes, the known *Spirulina* structure was used to create a molecular envelope for subsequent refinement of the protein phases by iterative molecular averaging and solvent flattening (Bricogne, 1976; Holden et al., 1987). The initial averaging was performed at 3.0-Å resolution for 15 cycles; the initial protein phases based on the single isomorphous heavy-atom derivative were discarded after the first cycle. The structure factor weighting algorithm used in the averaging process was of the form $w = e^{-(|F_o| - |F_c|)/|F_o|}$, where $|F_o|$ was the observed structure factor amplitude and $|F_c|$ was the calculated structure factor amplitude (Rayment, 1983). The resolution was extended to 2.5 Å in 0.1-Å increments by including the single isomorphous heavy-atom derivative phases for each new wedge of X-ray data for the first cycle, followed by 15 cycles of refinement at the corresponding resolution. The final R factor between the calculated structure factors from the averaged electron density map and the observed X-ray data was 19.3%. The resulting electron density map confirmed the choice of hand of the heavy-atom constellation in that the α-helices were right-handed.

An initial protein model was built on an Evans and Sutherland PS390 graphics system by using the averaged electron density map calculated from 30.0- to 2.5-Å resolution, the molecular modeling program FRODO (Jones, 1985), and the amino acid sequence based on the gene sequence (Alam et al., 1986). The model was then refined with a least-squares re-

Table IV: Refinement Statistics

resolution limits (Å)	30.0–2.5
initial R factor (%)[a]	47.3
final R factor (%)	18.7
no. of cycles of refinement and model building	42
no. of reflections used	7672
no. of atoms	1743
weighted root-mean-square deviations from ideality	
bond length (Å)	0.014
bond angle (deg)	2.6
planarity (trigonal) (Å)	0.011
planarity (other planes) (Å)	0.012
torsion angle (deg)[b]	24.775

[a] R factor $= \sum |F_o - F_c|/\sum |F_o|$. [b] The torsion angles were not restrained during the refinement.
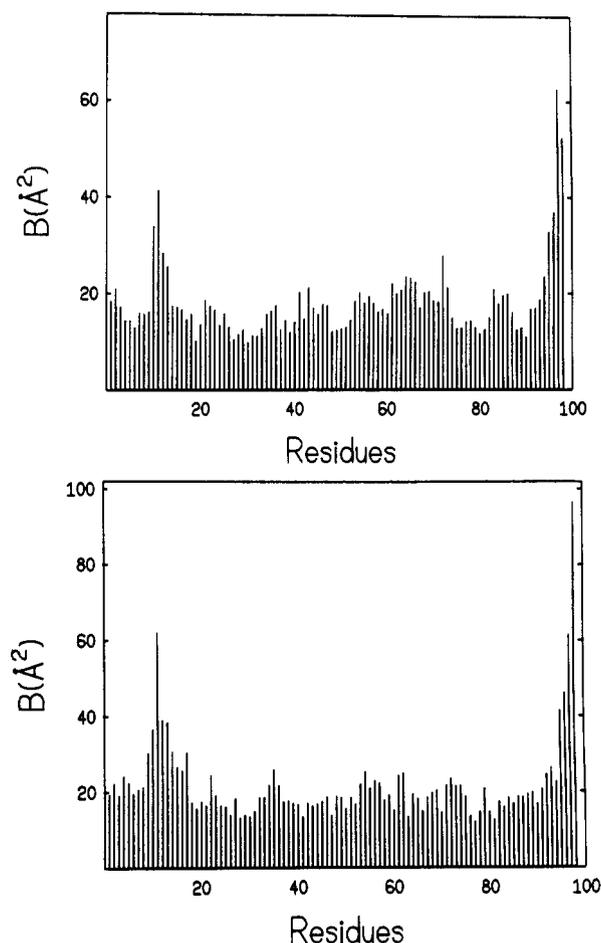

FIGURE 2: Plot of the mean main-chain B values versus amino acid residue number. Shown are (a) the mean main-chain temperature factors for one of the independent molecules in the asymmetric unit and (b) the mean main-chain temperature factors for the second molecule in the asymmetric unit.

finement package developed in Dr. Brian Matthews' laboratory (Tronrud et al., 1987). The initial R factor was 47.3%. After 42 cycles of alternate least-squares refinement and model building, the R factor was reduced to 18.7%. Both the positions and the temperature factors for the individual atoms were refined, and 235 solvent molecules were included in the refinement. Relevant refinement statistics are given in Table IV, and the distribution of the mean main-chain temperature factors are given in Figure 2.

RESULTS AND DISCUSSION

A representative portion of the electron density map is shown in Figure 3 and was calculated with coefficients of the form $(2F_o - F_c)$, where F_o is the native structure factor amplitude
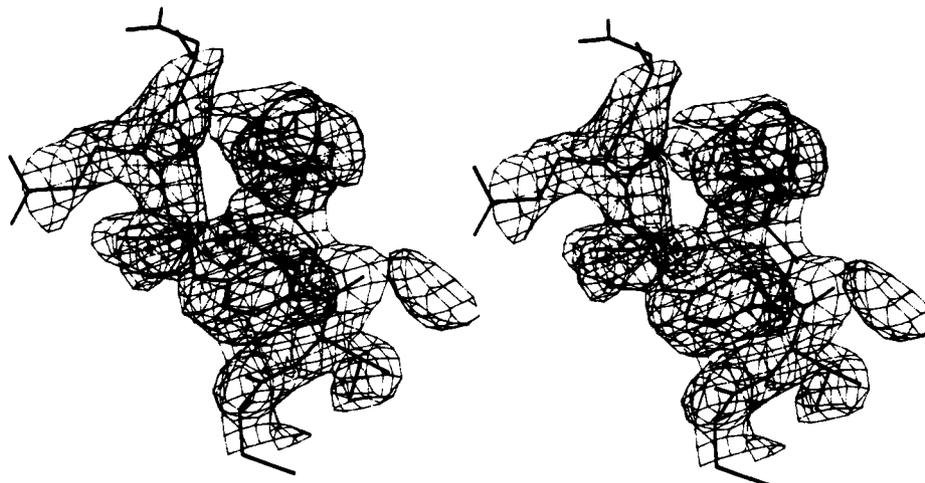
FIGURE 3: Representative portion of the electron density map calculated at 2.5-Å resolution. Shown is a portion of the electron density map calculated with coefficients of the form $(2F_o - F_c)$. The tyrosine models built into the electron density correspond to residues 25 and 82 in the ferredoxin amino acid sequence. Small spheres of electron density, indicated by crosses, correspond to ordered solvent molecules. The protein model was built by using an Evans and Sutherland PS390 graphics system and the molecular modeling program FRODO (Jones, 1985). The quality of the electron density displayed here is consistent throughout the entire protein map with the only exception being the C-terminal tyrosine residues for each molecule in the asymmetric unit.
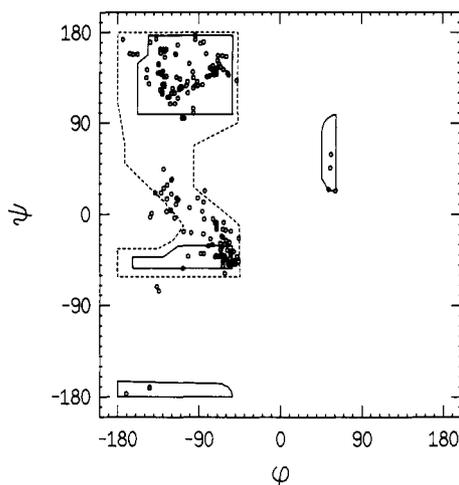

FIGURE 4: Ramachandran plot of all non-glycinyl main-chain dihedral angles for the ferredoxin model. Fully allowed ϕ,ψ values are enclosed by solid lines; those only partially allowed are enclosed by dashed lines. As can be seen from consideration of ϕ,ψ values, almost all the amino acid residues exhibit conformations that are typical for globular proteins. Approximately 44% of the amino acid residues adopt α-helical or β-sheet conformations; the other residues adopt "so-called" random coil configurations.

and F_c is the calculated structure factor amplitude. The electron density is well-defined for the two molecules within the asymmetric unit, except for each of the C-terminal tyrosine residues, which at this stage in the structural analysis appear to be disordered. A plot of the main-chain dihedral angles is given in Figure 4. The two molecules in the asymmetric unit superimpose with a root-mean-square value of 0.30 Å for α-carbon positions only.

As can be seen from the ribbon drawing in Figure 5 and the stereoview of an α-carbon model in Figure 6, the main secondary structural elements found in this ferredoxin include two α-helices (residues 26–32 and 68–73), a helical turn (residues 94–98), and four strands of β-pleated sheet [residues 1–9 (A), 14–20 (B), 51–54 (C), and 87–91 (D)]. The β-strands combine to form a mixed sheet, with strands A and B running antiparallel to one another and connected by a hairpin loop, with strands C and D running antiparallel but joined by a rather complicated crossover connection and with strands D and A running parallel to each other.
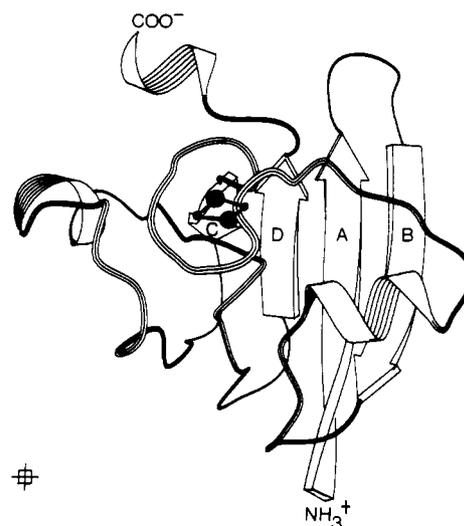

FIGURE 5: Ribbon drawing of the ferredoxin molecule. In this cartoon, strands of β-pleated sheet are shown as arrows, α-helices are shown as coils, and the [2Fe-2S] cluster is represented by a ball-and-stick model. The N and C termini are indicated, and the β-strands are labeled as described in the text. Although the figure lacks structural detail, it emphasizes the secondary structural elements found in this iron–sulfur protein. For example, in this drawing the mixed β-pleated sheet is immediately apparent. This figure was generated by using software kindly provided by Dr. J. P. Priestle.

As observed in the *Spirulina* ferredoxin structure (Tsukihara et al., 1981), the iron–sulfur cluster in the *Anabaena* molecule is located toward the outer edge of the molecule (Figure 6). A close-up view of the cluster binding site is shown in Figure 7. The two irons in the cluster are tetrahedrally coordinated by inorganic sulfurs and by sulfurs donated by cysteine residues 41, 46, 49, and 79. As shown in Figure 7, the two inorganic sulfur atoms in the cluster are within 3.3–3.4 Å of the amide nitrogens of residues Ser 40, Arg 42, Gly 44, Ala 45, and Cys 46; the sulfur atom of Cys 46 is within hydrogen-bonding distance (3.4 Å) of the amide nitrogen of Ser 47 and the side-chain oxygen atom of Thr 48; the sulfur atom of Cys 41 is within 3.3 Å of the amide nitrogens of Arg 42 and Ala 43; and, finally, the sulfur atom of Cys 79 is 3.4 Å from the amide nitrogen of Gly 44. It has been suggested that the extent of hydrogen bonding to the redox centers in electron-transport proteins may be one important modulator of oxidation–re-
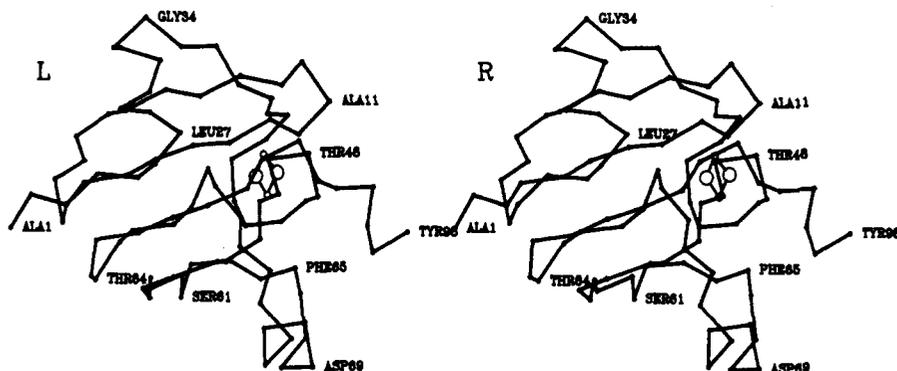
FIGURE 6: Stereoview of the α-carbon model of one of the ferredoxin molecules in the asymmetric unit. For simplicity only the positions of the α-carbons are represented. The iron–sulfur cluster is shown as an atomic model. Amino acid residues are labeled at various positions to aid the reader in following the course of the polypeptide chain. This figure was generated with the plotting software package PLUTO, originally written by Dr. Sam Motherwell and modified for proteins by Drs. Eleanor Dodson and Phil Evans.
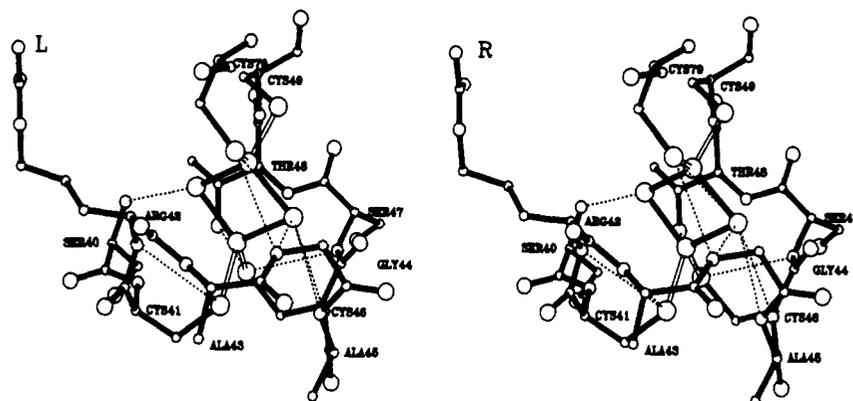

FIGURE 7: Close-up view of the iron–sulfur cluster binding site. Only those amino acid residues within approximately 3.5 Å of atoms in the metal cluster are shown. Potential hydrogen bonds from the protein to the inorganic sulfur atoms in the cluster and to the cysteine sulfurs are indicated by dashed lines; these range in length from 3.3 to 3.4 Å.
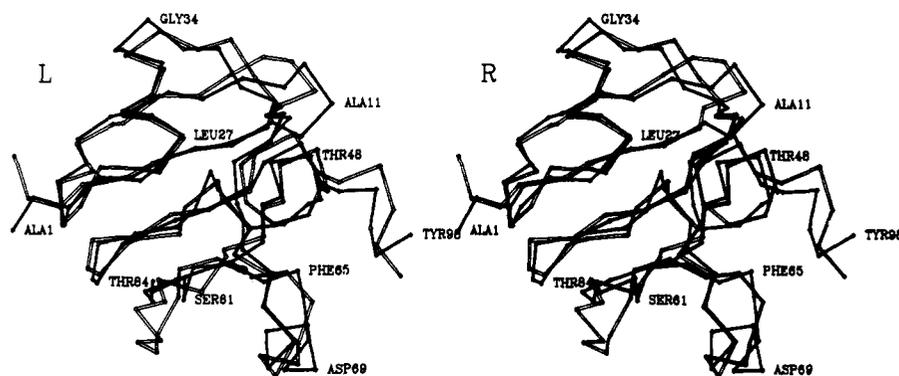

FIGURE 8: Superposition of the structure of the ferredoxins from *Spirulina* and *Anabaena*. The stereoview displays only the positions of the α-carbons. The *Anabaena* structure is shown in filled bonds, while the *Spirulina* fold is shown in open bonds. The major differences between these two molecules occur in the region located toward the bottom part of the figure.

duction potentials (Backes et al., 1991). Clearly, there are numerous potential hydrogen-bonding donors located near the iron–sulfur cluster in the *Anabaena* molecule. A detailed analysis of the hydrogen-bonding pattern, however, must await a higher resolution investigation.

Within recent years, it has been suggested that all plant-type ferredoxins have the same main-chain fold (Tsutsui et al., 1983). The molecules isolated from *Anabaena* and *Spirulina*, for example, contain 98 amino acid residues and are 80% homologous with respect to amino acid sequence. A comparison of the α-carbon positions for the *Anabaena* and the *Spirulina* molecules is shown in stereo in Figure 8. X-ray coordinates for the *Spirulina* protein were obtained from the Brookhaven Protein Data Bank (Bernstein et al., 1977). These

two ferredoxins were superimposed according to the algorithm described by Rossmann and Argos (1972). The positions of the α-carbons of the N-terminal residues differ by 6.1 Å although both are alanines. As can be seen from Figure 8, the hairpin loops connecting β-strands A and B (residues 10–14) also differ with a root-mean-square value of 2.8 Å for the positions of the α-carbon atoms. The amino acid sequences in this region are identical except for residue 14, which is a Thr in the *Anabaena* molecule and an Ile in the *Spirulina* ferredoxin. Large deviations between the two protein models begin at residue 53. In the regions delineated by residues 57–62, the root-mean-square difference between α-carbon positions is 6.6 Å, and yet the amino acid sequences in this region differ by only one residue (Val 58 in the *Anabaena*

protein and Ile 58 in the *Spirulina* molecule). Note that the root-mean-square difference between α-carbon positions in this region for the two independent molecules in the asymmetric unit of the *Anabaena* crystals is 0.17 Å. Also, in the refined *Anabaena* molecule, the average temperature factor for all main-chain backbone atoms in this region is 19.0 Å^2, suggesting that the region is not particularly "floppy". In addition, while both proteins have identical amino acid sequences between residues 67 and 73, this region is in an α-helical conformation in the *Anabaena* ferredoxin and appears as a random coil in the *Spirulina* protein. The average temperature factor for all main-chain backbone atoms in this helical region in the *Anabaena* molecule is 20.6 Å^2, again suggesting that the region is not especially flexible. The root-mean-square difference between α-carbon positions in this helical region for the two independent molecules in the asymmetric unit of the *Anabaena* crystals is 0.67 Å. It is important to note that these observed differences are most likely due to the fact that the *Spirulina* model has not been refined and consequently, the *Anabaena* model presented here is a more accurate description of the [2Fe-2S] ferredoxin fold.

In conclusion, the oxidized [2Fe-2S] ferredoxin isolated from the cyanobacterium *Anabaena* has been crystallized and its molecular structure solved and refined to 2.5-Å resolution. The basic overall fold is similar to the homologous ferredoxin from *Spirulina*, but the two molecules differ in several regions, which may be due to the fact that the original model for the *Spirulina* protein has not been refined. The X-ray coordinates of the *Anabaena* ferredoxin have been deposited in the Brookhaven Protein Data Bank, and they may also be obtained via HOLDEN @ VMS.MACC.WISC.EDU (INTERNET) or HOLDEN @ WISCMACC (BITNET).

REFERENCES

Aketagawa, J., & Tamura, G. (1980) *Agric. Biol. Chem. 44,* 2371-2378.

Alam, J., Whitaker, R. A., Krogmann, D. W., & Curtis, S. E. (1986) *J. Bacteriol. 168,* 1265-1271.

Backes, G., Mino, Y., Loehr, T. M., Meyer, T. E., Cusanovich, M. A., Sweeney, W. V., Adman, E. T., & Sanders-Loehr, J. (1991) *J. Am. Chem. Soc. 113,* 2055-2064.

Beinert, H. (1973) *Iron-Sulfur Proteins* (Lovenberg, W., Ed.) Vol. 1, pp 1-36, Academic Press, New York.

Beinert, H. (1990) *FASEB J. 4,* 2483-2491.

Bernstein, F. C., Koetzle, T. F., Williams, G. J. B., Meyer, E. F., Jr., Brice, M. D., Rogers, J. R., Kennard, O., Shimanouchi, T., & Tasumi, M. (1977) *J. Mol. Biol. 112,* 535-542.

Bricogne, G. (1976) *Acta Crystallogr. A32,* 832-847.

Cammack, R., Roa, K. K., Bargeron, C. P., Hutson, K. G., Andrew, P. W., & Rogers, L. J. (1977) *Biochem. J. 168,* 205-209.

Holden, H. M., Rypniewski, W. R., Law, J. H., & Rayment, I. (1987) *EMBO J. 6,* 1565-1570.

Ida, S. (1977) *J. Biochem. 82,* 915-918.

Jones, T. A. (1985) *Methods Enzymol. 115,* 157-171.

Lea, P. J., & Miflin, B. J. (1974) *Nature 251,* 614-616.

Masaki, R., Yoshikawa, S., & Matsubara, H. (1982) *Biochim. Biophys. Acta 700,* 101-109.

Oh, B.-H., & Markley, J. L. (1990) *Biochemistry 29,* 3993-4004.

Rayment, I. (1983) *Acta Crystallogr. A39,* 102-116.

Rossmann, M. G. (1960) *Acta Crystallogr. 13,* 221-226.

Rossmann, M. G. (1979) *J. Appl. Crystallogr. 12,* 225-238.

Rossmann, M. G., & Argos, P. (1975) *J. Biol. Chem. 250,* 7525-7532.

Schmid, M. F., Weaver, L. H., Holmes, M. A., Grutter, M. G., Ohlendorf, D. H., Reynolds, R. A., Remington, S. J., & Matthews, B. W. (1981) *Acta Crystallogr. A37,* 701-710.

Sussman, J. L., Brown, J. H., & Shoham, M. (1986) *Iron-Sulfur Protein Research* (Matsubara et al., Eds.) pp 69-82, Japan Sci. Soc. Press, Tokyo/Springer-Verlag, Berlin.

Terwilliger, T. C., & Eisenberg, D. (1983) *Acta Crystallogr. A39,* 813-817.

Thomson, A. J. (1985) *Metalloproteins Part I, Metal Proteins with Redox Roles* (Harrison, P., Ed.) pp 79-120, Verlag Chemie, Weinheim, FRG.

Trebst, A., & Avron, M., Eds. (1977) *Photosynthesis I, Photosynthetic Electron Transport and Photophosphorylation,* Springer-Verlag, New York.

Tronrud, D. E., Ten Eyck, L. F., & Matthews, B. W. (1987) *Acta Crystallogr. A43,* 489-501.

Tsukihara, T., Fukuyama, K., Nakamura, M., Katsube, Y., Tanaka, N., Kakudo, M., Wada, K., Hase, T., & Matsubara, H. (1981) *J. Biochem. 90,* 1763-1773.

Tsutsui, T., Tsukihara, T., Fukuyama, K., Katsube, Y., Hase, T., Matsubara, H., Nishikawa, Y., & Tanaka, N. (1983) *J. Biochem. 94,* 299-302.